



An edge-based smoothed finite element method (ES-FEM) for analyzing three-dimensional acoustic problems

Z.C. He^{a,b,*}, G.R. Liu^{b,c}, Z.H. Zhong^a, S.C. Wu^{b,d}, G.Y. Zhang^c, A.G. Cheng^a

^aState Key Lab. of Advanced Technology for Vehicle Body Design and Manufacture, Hunan University, Changsha 410082, PR China

^bCentre for Advanced Computations in Engineering Science (ACES), Department of Mechanical Engineering, National University of Singapore, 9 Engineering Drive 1, 117576 Singapore, Singapore

^cSingapore-MIT Alliance (SMA), E4-04-10, 4 Engineering Drive 3, 117576 Singapore, Singapore

^dCentre for Advanced Materials Processing and Simulations, School of Materials Science and Engineering, Hefei University of Technology, Hefei 230009, PR China

ARTICLE INFO

Article history:

Received 29 July 2008

Received in revised form 10 September 2009

Accepted 10 September 2009

Available online 17 September 2009

Keywords:

Acoustic

Numerical method

Meshfree method

Finite element method (FEM)

Edge-based smoothed finite element method (ES-FEM)

Discretization error

ABSTRACT

It is well-known that one key issue of solving the Helmholtz equation using finite element method (FEM) is the accuracy deterioration in the solution with increasing wave number due to the “numerical dispersion error”. Such a numerical dispersion error is essentially caused by the “overly-stiff” nature of the FEM model. To overcome this problem, this paper presents an edge-based smoothed finite element method (ES-FEM) for analyzing acoustic problems using linear triangular and tetrahedron elements that can be generated automatically, respectively, for complicated two-dimensional and three-dimensional domains. The discretized linear system equations for ES-FEM are established using the smoothed Galerkin weak form with smoothing domains associated with the edges of the triangles or surfaces of the tetrahedrons. The edge-based gradient smoothing operation provides proper softening effect, makes the ES-FEM model much softer than the “overly-stiff” FEM model and hence significantly reduces the numerical dispersion error. Numerical examples, including a 2D problem of acoustic pressure distribution in a vehicle passenger compartment and a 3D problem about the acoustic pressure distribution in an engine chamber, have been studied using the present ES-FEM. The results demonstrate that the ES-FEM possesses the following advantages compared with the standard FEM using the same meshes. First, ES-FEM achieves similar convergence rate but better accuracy especially at high frequency. Second, ES-FEM is less sensitive to the mesh distortion, meaning that the quality of mesh has less effect on the solution of ES-FEM. Third, it works well for triangular types of meshes, and thus for the problems with complicated geometry.

© 2009 Elsevier B.V. All rights reserved.

1. Introduction

During the past several decades, many numerical methods have been introduced to compute the approximate solutions of acoustic, aeroacoustic and structural-acoustic problems [1–4,27–29]. The standard finite element method (FEM) and boundary element method (BEM) are the most well-developed and widely-used numerical methods in solving these acoustic problems. A well-known issue of solving acoustic problems governed by the Helmholtz equation with numerical methods including FEM is the so-called “numerical dispersion” errors, i.e. error on the phase of the numerically simulated waves [1], in addition to the usual “interpolation error”. In the low frequency range, the numerical methods can provide appropriate results; in the higher frequency range, the numerical dispersion error can not be negligible any more unless a sufficiently (beyond the usual rule-of-thumb) fine

mesh is used. However, such an extra fine mesh will lead to a dramatic increase of computational cost, especially for large scale 3D acoustic problems.

In order to overcome the problem of numerical dispersion error, various techniques have been proposed to tackle the numerical pollution of FEM. Reference [3] showed that the high-order elements and the QSFEM (Quasi Stabilized FEM) are effective in lowering the dispersion error, but the QSFEM is very complicated in the general setting. Petersen et al. [4] assessed the efficiency of currently available shape function families, such as the conventional Lagrange functions, various p -FEM shapes, and spectral element shape functions. It showed that the higher-order polynomial shape approximations lead to more accurate solutions and Bernstein polynomials provide the most efficient and stable solution. Another approach is the Galerkin/least-squares finite element method (GLS) [5] with a stabilization term for Helmholtz equations. The same idea has been applied in aeroacoustics with algebraic subgrid scale (ASGS) approach for the convected Helmholtz equation [6]. In recent years, meshfree methods have been developed

* Corresponding author. Tel./fax: +86 73188822051.

E-mail address: hezicheng815@gmail.com (Z.C. He).

and applied to many engineering problems. The element-free Galerkin method (EFGM), introduced by Belytschko et al. [7], has also been adopted to solve acoustic problems. Bouillard [8] showed that the EFGM is also affected by the dispersion and pollution phenomena, but these effects are relatively low compared to FEM. Alvarez et al. [9] used discontinuous finite element formulation for acoustic problems and found significant improvement in accuracy, but higher cost in computation. However, it is the authors' opinion that producing a properly "softened" stiffness for the discrete model is much more essential to the root of the numerical dispersion error.

Recently, strain smoothing techniques have been applied by Chen et al. [10] to stabilize the solutions of nodal integrated mesh-free methods and also in the natural-element method [11]. A linearly conforming point interpolation method (LC-PIM) has been formulated by using the node-based strain smoothing domains and the point interpolation method (PIM) for field variable approximation [12]. The PIM shape functions are constructed based on a small set of nodes in a local support domain and possess the Delta function property, which allows straightforward imposition of essential boundary conditions [13]. Because of the incompatible nature of the PIM shape functions, a generalization to the smoothing operation is needed [14]. Instead of using compatible strains obtained from the strain-displacement relation, LC-PIM uses the generalized smoothing technique to construct the strain field over node-based smoothing domains, ensuring the stability and convergence, providing softening effect to the model and significantly improving the accuracy. More importantly, it has been found that LC-PIM can provide upper bound solution in energy norm for elasticity problems with homogeneous essential boundary conditions [15].

Because the node-based domains are used, LC-PIM is also termed as node-based smoothed point interpolation method (or NS-PIM). Applying the strain smoothing technique to the finite element setting, the node-based smoothed finite element method (NS-FEM) has also been formulated and applied to triangular, 4-node quadrilateral and n -sided polygonal elements [16]. When 3-node triangular elements are used, the NS-FEM is identical to the NS-PIM using linear PIM shape functions and hence also possesses the upper bound property [16]. However, NS-PIM and NS-FEM models behave "overly-soft" leading to temporal instability problems observed as spurious non-zero energy modes in vibration analysis [14,17]. Techniques such as the alpha finite element method (α FEM) are needed to eliminate this instability issue [19]. The edge-based smoothed finite element method (ES-FEM) and the edge-based smoothed point interpolation method (ES-PIM) have therefore been proposed with the strain smoothing operated over the edge-based smoothing domains in FEM and meshfree settings [17,18]. In one-dimensional (1D) problems, the ES-FEM is the same as NS-FEM encountering instability problems. While in two-dimensional (2D) problems, the ES-FEM is found to be stable (no spurious non-zero energy modes), exhibits neither "overly-stiff" nor "overly-soft" behaviors and can hence achieve much more accurate results [14,17]. The similar features are also found in the 3D version of ES-FEM, i.e. the face-based smoothed FEM or FS-FEM [20], and the plate formulation [21].

Owing to the properly softened stiffness of the model, it is natural to expect that the ES-FEM will greatly reduce the numerical dispersion error and obtain accurate results for acoustic problems. We, therefore, further formulate the ES-FEM for solving acoustic problems in both 2D and 3D domains in the present work. The smoothed Galerkin weak form is used to derive the discretized linear system equations; the numerical integration and gradient smoothing operation are applied over the edge/face-based smoothing domains. A number of numerical examples have been studied, which include two problems with analytical solutions, a 2D practi-

cal problem of a vehicle passenger compartment and a 3D problem of acoustic pressure distribution in an engine chamber. All the numerical results show that the present method is stable and can provide more accurate results compared with the standard FEM using the same mesh.

The paper is organized as follows: Section 2 briefly describes the mathematical model. Section 3 introduces the detailed formulation of the edge-based smoothed finite element method for acoustic problems. Section 4 outlines the issue of controlling the numerical dispersion error. In Section 5, a number of examples are studied in detail. Finally, the conclusions from the numerical results are presented in Section 6.

2. Mathematical model of acoustic problems

Consider an acoustic problem domain Ω with boundary Γ and the boundary is decomposed into three portions Γ_D, Γ_N and Γ_A , which $\Gamma = \Gamma_D \cup \Gamma_N \cup \Gamma_A$. The Dirichlet, Neumann and admittance (Robin) boundary conditions are prescribed on Γ_D, Γ_N and Γ_A , respectively. Let p' denote the field acoustic pressure and c is the speed of sound traveling in the fluid. The acoustic wave equation can be written as follows:

$$\Delta p' - \frac{1}{c^2} \frac{\partial^2 p'}{\partial t^2} = 0 \quad \text{in } \Omega, \quad (1)$$

where Δ and t denote the Laplace operator and time, respectively. Here we assume that the acoustic pressure p' is a small harmonic perturbation around a steady state in the fluid. The acoustic pressure can then be expressed as:

$$p' = p e^{i\omega t}, \quad (2)$$

where $j = \sqrt{-1}$, ω is the angular frequency and the p is the amplitude of the acoustic wave. In general, the acoustic pressure p is complex-valued in the frequency domain, and satisfies the Helmholtz equation given by:

$$\Delta p + k^2 p = 0, \quad (3)$$

where k is the wave number defined by

$$k = \frac{\omega}{c}. \quad (4)$$

The Dirichlet, Neumann and admittance (Robin) boundary conditions on Γ_D, Γ_N and Γ_A can be described as follows:

$$p = p_D \quad \Gamma_D \quad \text{Dirichlet condition}, \quad (5)$$

$$v = v_n \quad \text{or} \quad \nabla p \cdot n = -j\rho\omega v_n \quad \Gamma_N \quad \text{Neumann condition}, \quad (6)$$

$$v = A_n p \quad \text{or} \quad \nabla p \cdot n = -j\rho\omega A_n p \quad \Gamma_A \quad \text{Robin condition}, \quad (7)$$

where v_n, ρ and A_n represent the normal velocity on the boundary Γ_N , the density of medium and the admittance coefficient on boundary Γ_A , respectively.

The acoustic particle velocity v in ideal fluid is linked to the gradient of acoustic pressure p by the equation of harmonic motion which can be expressed:

$$\nabla p + j\rho\omega v = 0. \quad (8)$$

3. Formulation of the ES-FEM

3.1. Discretized system equations

We first brief the standard weak formulation for acoustic problems. The weighted residual equation is first obtained by multiplying Eq. (1) with a test function w in the entire domain and can be written as:

$$\int_{\Omega} w(\Delta p + k^2 p) d\Omega = 0. \quad (9)$$

Integrating by parts and using Green's theorem, we have

$$-\int_{\Omega} \nabla w \cdot \nabla p d\Omega + k^2 \int_{\Omega} w \cdot p d\Omega + \int_{\Gamma} w(\nabla p \cdot \mathbf{n}) d\Gamma = 0. \quad (10)$$

Applying the boundary conditions shown in Eqs. (5)–(7), we obtain

$$\begin{aligned} & -\int_{\Omega} \nabla w \cdot \nabla p d\Omega + k^2 \int_{\Omega} w \cdot p d\Omega - j\rho\omega \int_{\Gamma_N} w \cdot v_n d\Gamma \\ & - j\rho\omega A_n \int_{\Gamma_A} w \cdot p d\Gamma = 0. \end{aligned} \quad (11)$$

In the above weighted residual form, the field variable pressure can be expressed in the approximate form:

$$p = \sum_{i=1}^m N_i p_i = \mathbf{N} \mathbf{p}, \quad (12)$$

where N_i are FEM shape functions and p_i is the unknown nodal pressure. In standard Galerkin weak form the shape function \mathbf{N} is also used as the weight function w and the weak form for acoustic problem can be obtained as:

$$\begin{aligned} & -\int_{\Omega} \nabla \mathbf{N} \cdot \nabla \mathbf{N} p d\Omega + k^2 \int_{\Omega} \mathbf{N} \cdot \mathbf{N} p d\Omega - j\rho\omega \int_{\Gamma_N} \mathbf{N} \cdot v_n d\Gamma \\ & - j\rho\omega A_n \int_{\Gamma_A} \mathbf{N} \cdot \mathbf{N} p d\Gamma = 0. \end{aligned} \quad (13)$$

Introducing the gradient smoothing technique based on edges of elements [17] or faces of elements [19], the gradient component $\nabla \mathbf{N}$ is replaced by the smoothed item $\overline{\nabla \mathbf{N}}$, the smoothed Galerkin weak form for acoustic problem can be written as:

$$\begin{aligned} & -\int_{\Omega} \overline{\nabla \mathbf{N}} \cdot \overline{\nabla \mathbf{N}} p d\Omega + k^2 \int_{\Omega} \mathbf{N} \cdot \mathbf{N} p d\Omega - j\rho\omega \int_{\Gamma_N} \mathbf{N} \cdot v_n d\Gamma \\ & - j\rho\omega A_n \int_{\Gamma_A} \mathbf{N} \cdot \mathbf{N} p d\Gamma = 0. \end{aligned} \quad (14)$$

The discretized system equations can be finally obtained and written in the following matrix form:

$$[\overline{\mathbf{K}} - k^2 \mathbf{M} + j\rho\omega \mathbf{C}] \{\mathbf{P}\} = -j\rho\omega \{\mathbf{F}\}, \quad (15)$$

where

$$\overline{\mathbf{K}} = \int_{\Omega} (\overline{\nabla \mathbf{N}})^T \overline{\nabla \mathbf{N}} d\Omega \quad \text{The acoustical stiffness matrix,} \quad (16)$$

$$\mathbf{M} = \int_{\Omega} \mathbf{N}^T \mathbf{N} d\Omega \quad \text{The acoustical mass matrix,} \quad (17)$$

$$\mathbf{C} = \int_{\Gamma_A} \mathbf{N}^T \mathbf{N} A_n d\Gamma \quad \text{The acoustical damping matrix,} \quad (18)$$

$$\mathbf{F} = \int_{\Gamma_N} \mathbf{N}^T v_n d\Gamma \quad \text{The vector of nodal acoustic forces,} \quad (19)$$

$$\{\mathbf{P}\}^T = \{p_1, p_2, \dots, p_n\} \quad \text{Nodal acoustic pressure in the domain.} \quad (20)$$

To obtain Eq. (16), the numerical integration procedure is performed based on the smoothing domains associated with the edges of the triangles in 2D [17] or surfaces of tetrahedrons in 3D [19].

3.2. Numerical integration with edge-based gradient smoothing operation

This section formulates the gradient smoothing domains of ES-FEM for 2D and 3D problems using triangular elements and tetrahedral elements, respectively. The formulation is almost the same for any other 2D and 3D n -side polygonal elements as long as the

simple point interpolation method is used to create shape functions [23].

In the process of numerical integration of ES-FEM for 2D problems, a mesh of 3-node triangles is generated first, which can be done easily and automatically using any mesh generator. Afterwards, the problem domain Ω is further divided into N smoothing domains associated with edges of the triangles such that $\Omega_1 \cup \Omega_2 \cup \dots \cup \Omega_N = \Omega$ and $\Omega_i \cap \Omega_j = \emptyset, i \neq j$, where N is the number of total edges of triangles. As shown in Fig. 1a, the smoothing domain Ω_k for edge k is created by connecting sequentially the end-points of edge k to the centroids of the neighbor triangles. Extending the smoothing domain Ω_k in 3D problems, the domain discretization is the same as that of standard FEM using tetrahedral elements and the smoothing domains are formed associated with the faces of tetrahedrons. As shown in Fig. 1b, the smoothing domain Ω_k for face k is created using the neighbor tetrahedral elements by connecting vertexes of the triangle (face k) to the centroids of two adjacent elements. The boundary of the smoothing domain Ω_k for edge k (or face k) is labeled as Γ_k and the union of all Ω_k form the global domain Ω exactly. To perform the numerical integration based on the smoothing domains, Eq. (16) can be further rewritten as:

$$\overline{\mathbf{K}} = \sum_{k=1}^N \overline{\mathbf{K}}^{(k)}, \quad (21)$$

in which

$$\overline{\mathbf{K}}^{(k)} = \int_{\Omega_k} \overline{\mathbf{B}}^T \overline{\mathbf{B}} d\Omega. \quad (22)$$

In the present method, smoothing operation is applied over each smoothing domain on the velocity v , which is linked to the gradient of acoustic pressure. The smoothed velocity can be obtained as:

$$\bar{v}(\mathbf{x}_k) = \int_{\Omega_k} v(\mathbf{x}_k) \overline{\mathbf{W}}(\mathbf{x} - \mathbf{x}_k) d\Omega, \quad (23)$$

where $\overline{\mathbf{W}}$ is a smoothing function given by

$$\overline{\mathbf{W}}(\mathbf{x} - \mathbf{x}_k) = \begin{cases} 1/V_k & \mathbf{x} \in \Omega_k, \\ 0 & \mathbf{x} \notin \Omega_k, \end{cases} \quad (24)$$

where $V_k = \int_{\Omega_k} d\Omega$ is the area of smoothing domain for edge k in 2D problems. When it comes to 3D problems, the V_k is the volume of smoothing domain for face k .

Substituting Eq. (24) into Eq. (23) and applying the Green's theorem, the smoothed field gradient (the smoothed velocity) can be obtained in terms of acoustic pressure:

$$\begin{aligned} \bar{v}(\mathbf{x}_k) &= \frac{1}{V_k} \int_{\Omega_k} v(\mathbf{x}) d\Omega = -\frac{1}{j\rho\omega V_k} \int_{\Omega_k} \nabla p d\Omega \\ &= -\frac{1}{j\rho\omega V_k} \int_{\Gamma_k} p \cdot \mathbf{n} d\Gamma. \end{aligned} \quad (25)$$

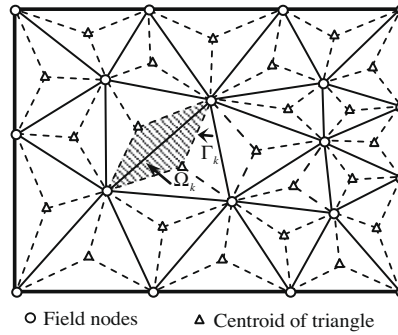
Using FEM shape function for field variable interpolation in the form of Eq. (12), the smoothed velocity for edge k can be written in the following matrix form.

$$\bar{v}(\mathbf{x}_k) = -\frac{1}{j\rho\omega} \sum_{i \in M_k} \overline{\mathbf{B}}_i(\mathbf{x}_k) p_i, \quad (26)$$

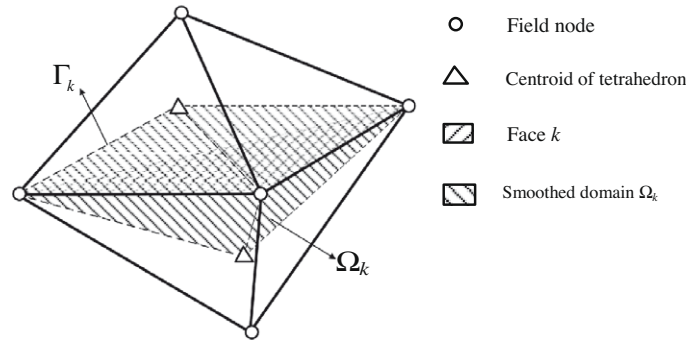
where M_k is the total number of nodes in the influence domain of edge k . For two-dimensional space

$$\overline{\mathbf{B}}_i^T(\mathbf{x}_k) = [\bar{b}_{i1} \quad \bar{b}_{i2}] \quad (\text{for 2D problem}), \quad (27)$$

$$\bar{b}_{ip} = \frac{1}{V_k} \int_{\Gamma_k} \mathbf{N}_i(\mathbf{x}) n_p(\mathbf{x}) d\Gamma \quad (p = 1, 2, \text{ for 2D problem}), \quad (28)$$



(a) Edge-based smoothing domains in 2D problem for gradient smoothing and integration are created by sequentially connecting the centroids of the adjacent triangles with the end-points of the edge.



(b) For 3D problems, the smoothing domain is created using the neighbor tetrahedral elements by connecting vertexes of the triangle (face k) to the centroids of two adjacent elements.

Fig. 1. Illustration of construction of smoothing domain for 2D and 3D problems.

and for three-dimensional space

$$\bar{\mathbf{B}}_i^T(\mathbf{x}_k) = [\bar{b}_{i1} \ \bar{b}_{i2} \ \bar{b}_{i3}] \quad (\text{for 3D problem}), \quad (29)$$

$$\bar{b}_{ip} = \frac{1}{V_k} \int_{\Gamma_k} N_i(\mathbf{x}) n_p(\mathbf{x}) d\Gamma \quad (p = 1, 2, 3, \text{ for 3D problem}), \quad (30)$$

where N_i is the FEM shape function for node i .

Using Gauss integration along each segment (or each surface triangle for 3D) of boundary Γ_k of the smoothing domain Ω_k , the above equations can be rewritten in the following summation forms as

$$\bar{b}_{ip} = \frac{1}{V_k} \sum_{q=1}^{N_s} \left[\sum_{r=1}^{N_g} w_r N_i(\mathbf{x}_{qr}) n_p(\mathbf{x}_q) \right], \quad (31)$$

where N_s is the number of segments of the boundary Γ_k (or number of surface triangles of 3D smoothing domain), N_g is the number of Gauss points distributed in each segment (or each surface triangle), and w_r is the corresponding weight for the Gauss point. The smoothed stiffness matrix shown in Eq. (22) can be calculated as:

$$\bar{\mathbf{K}}^{(k)} = \int_{\Omega_k} \bar{\mathbf{B}}^T \bar{\mathbf{B}} d\Omega = \bar{\mathbf{B}}^T \bar{\mathbf{B}} V_k. \quad (32)$$

It can be easily seen from Eq. (32) that the resultant linear system is symmetric and banded (due to the compact supports of FEM shape functions), which implies that the system equations can be solved efficiently.

4. Discretization error

It is well-known that the major concern of computing acoustic problems using FEM is to control the discretization error. The reason is that the numerical waves of FEM are dispersive, that is, the

wave number of the FEM solution is bound to be different from the wave number of exact solution [3]. There is so-called “the rule of thumb” which provides the minimum number of elements that are required per wavelength to obtain a stabilized solution to the Helmholtz equation. However, the error of numerical solutions often grows with the increase of wave number even if the rule of thumb is followed.

The gradient of acoustic pressure p is usually used as the *global error indicator* for the numerical computation. Based on the relation between the pressure and velocity described in Eq. (8), the numerical error indicator in terms of velocity can be expressed by:

$$e_n^2 = \int_{\Omega} (\bar{v}^{exact} - \tilde{v}^h)^T (v^{exact} - v^h) d\Omega, \quad (33)$$

where \bar{v} is complex conjugate of the velocity v , the superscript *exact* denotes the exact solutions and h denotes the numerical solutions obtained from numerical methods including the present ES-FEM and FEM.

Ihlenburg et al. show that the error can be estimated and the *relative error* for a uniform hp -mesh of finite element method is bounded by [24]:

$$\begin{aligned} \eta = \frac{e_n}{e_e} &= \sqrt{\frac{\int_{\Omega} (\bar{v}^{exact} - \tilde{v}^h)^T (v^{exact} - v^h) d\Omega}{\int_{\Omega} (\bar{v}^{exact} \cdot v^{exact})^2 d\Omega}} \\ &\leq C_1 \left(\frac{kh}{p}\right)^p + C_2 k \left(\frac{kh}{p}\right)^{2p}, \end{aligned} \quad (34)$$

where C_1 and C_2 are constant independent of the parameters k and h , and p here is the degree of polynomial approximation used in the numerical methods. The relative error contains two terms: the first term is *interpolation error* which defines the difference between the interpolation and the exact solution; the second term is generally

known as *numerical dispersion error* which relates to the error in the numerical wave number. For linear interpolation ($p = 1$) discussed here, it is shown in Refs. [25,26] that if $kh < 1$, the relative error for acoustic problems can be expressed by:

$$\eta \leq C_1 kh + C_2 k^3 h^2, \tag{35}$$

From the expression above, it can be found that the error strongly depends on the *wave number* k and *mesh size* h . The *interpolation error* can be controlled by keeping kh a constant. This is the “the rule of thumb” which prescribes the relation between the wave number and mesh size. Even according to the classical rule, it is not sufficient to control the numerical dispersion error because it will increase linearly with the increase of k .

In this work, “the rule of thumb” is also observed by the present ES-FEM. Compared with the overly-stiff FEM model, the ES-FEM model with properly softened stiffness will reduce the numerical dispersion error and hence obtain more accurate solutions. The numerical results of a number of examples will demonstrate this point.

5. Numerical examples

In this paper, two examples with analytical solutions, a 2D problem of a car passenger compartment and a 3D problem of an

engine chamber are studied in detail to investigate the accuracy and convergence of the ES-FEM. Suppose l is the length of the study domain, the Cartesian two-dimensional coordinates are characterized by two variables x and y , the non-dimensional coordinates are defined by:

$$\xi = x/l, \quad \zeta = y/l. \tag{36}$$

So the wave number k and mesh size h in the Section 5.1 and 5.2 are also expressed in a non-dimensional wave number κ and size h

$$\kappa = kl, \quad h = h/l. \tag{37}$$

5.1. 1D problem with Dirichlet boundary condition

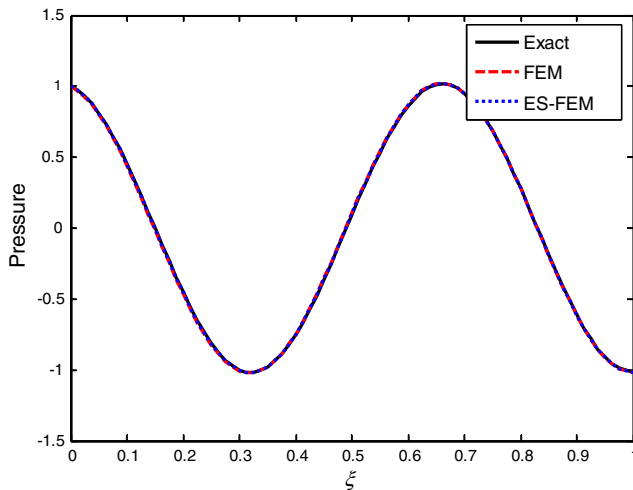
Consider a time-harmonic wave propagates in the domain $\Omega = (0, 1)$ with Dirichlet and Neumann boundary conditions described as follows:

$$\frac{d^2 p}{d\xi^2} + \kappa^2 p = 0 \quad \text{in } \Omega(0 \leq \xi \leq 1), \tag{38}$$

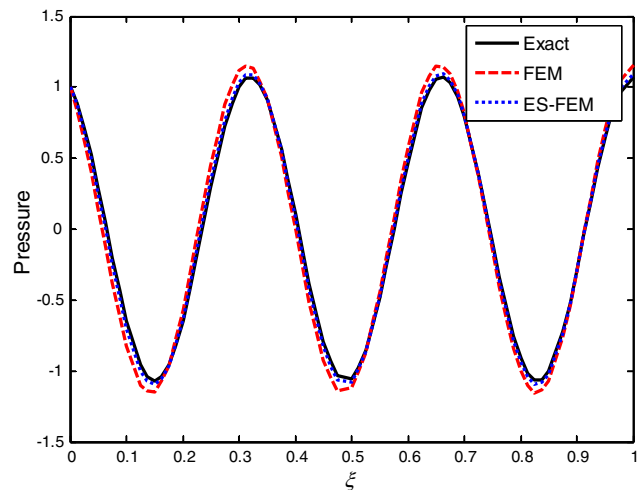
$$p(0) = 1, \quad \frac{dp}{d\xi}(1) = 0. \tag{39}$$

The problem has an analytical solution as follows:

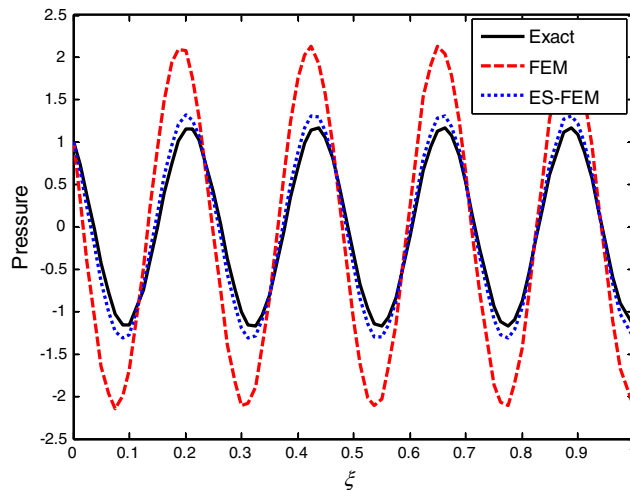
$$p(\xi) = \cos(\kappa\xi) + \tan \kappa \sin(\kappa\xi). \tag{40}$$



(a) 500Hz



(b) 1000Hz



(c) 1500Hz

Fig. 2. Exact and numerical solutions of acoustic pressure at different frequency values for the 1D time-harmonic problem.

For simplicity, the density of fluid is 0.004 kg/m³ and the velocity of the wave is 340 m/s. Three different frequency values (500 Hz ($\kappa = 9.24$), 1000 Hz ($\kappa = 18.48$), 1500 Hz ($\kappa = 27.72$)) have been employed to study the problem using ES-FEM with mesh size of 0.03. For the purpose of comparison, FEM solutions are also computed using the same triangle mesh as well as in the ES-FEM. The numerical results of acoustic pressure using ES-FEM and FEM at different frequency values, together with the exact solutions, are plotted in Fig. 2. It can be seen from these plots that:

1. For the problem at low frequency (small wave number), as shown in Fig. 2a, ES-FEM and FEM give similar results which are all in good agreement with the exact solution.
2. With the increase of frequency, the numerical solutions of both ES-FEM and FEM will depart from the exact one. Compared to FEM, the ES-FEM can provide much better results, thanks to the very quickly softened stiffness of the model.

The convergence and accuracy property of ES-FEM are then investigated at 500 Hz ($\kappa = 9.24$), 1000 Hz ($\kappa = 18.48$) and 1500 Hz ($\kappa = 27.72$) using four types of uniformly distributed

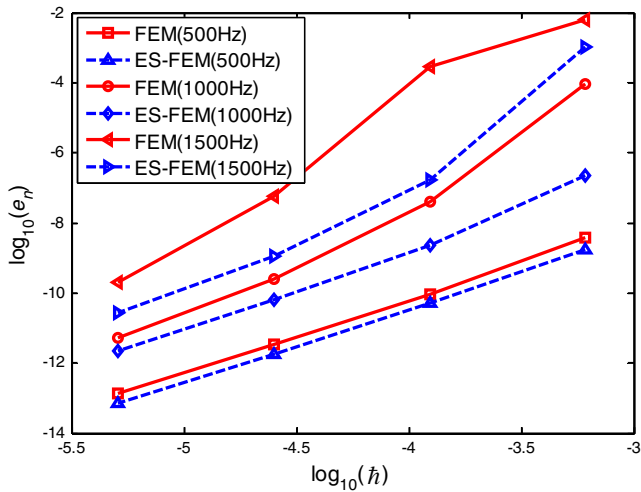


Fig. 3. Comparison of accuracy and convergence property at different frequency values between ES-FEM and FEM.

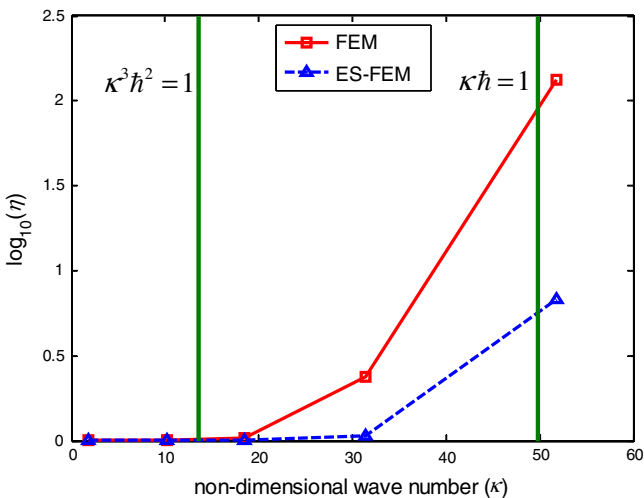


Fig. 4. Relative error changing with non-dimensional wave number based on the same mesh.

nodes (103, 365, 1369, 5297 nodes, respectively). The results obtained from the ES-FEM and FEM in terms of global error are plotted together in Fig. 3. From this figure it can be found that at low frequency (500 Hz), ES-FEM obtains similar accuracy and convergence rate compared with FEM; with the increase of frequency, ES-FEM can achieve better accuracy. These results show clearly that the error of the ES-FEM solution is less sensitive and more stable than the FEM with respect to the increase of frequency. This finding is inline with our predictions based on the theorem and formulation of ES-FEM.

The sensitivity of the relative error against non-dimensional wave number has also been investigated with constant mesh size and a comparison of the numerical results between the ES-FEM and FEM is depicted in Fig. 4. The interpolation error (κh) and numerical dispersion error ($\kappa^3 h^2$) are called pre-asymptotic and asymptotic estimate [25], respectively. Cases of the $\kappa h = 1$ and $\kappa^3 h^2 = 1$ are also presented in Fig. 4. It can be concluded that the relative errors at low wave numbers obtained from FEM and ES-FEM are both small. With the increase of non-dimensional wave number, the relative errors increase dramatically for both methods, but the relative errors of present ES-FEM are much smaller than that of FEM solutions. These findings again show that ES-FEM is less sensitive to non-dimensional wave number than FEM does.

5.2. 2D problem with Neumann boundary condition

Another problem is a 2D tube filled with water as shown in Fig. 5. The dimension of this tube with length $l = 1$ m and width $b = 0.1$ m is considered. The left of the tube is excited by the harmonic motion with normal velocity $v_n = 10 \sin \omega t$, the right end of the tube is rigid wall and the normal velocity $v = 0$ m/s. The density of water ρ is 1000 kg/m³ and the speed of sound in the water is 1500 m/s. The analytical solutions for this problem can be easily derived and the pressure and velocity are given by

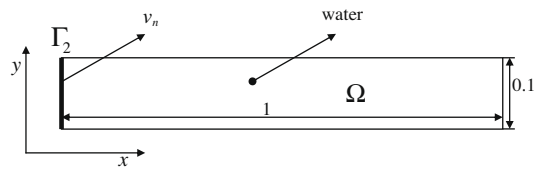


Fig. 5. 1D acoustic chamber with the Neumann boundary condition.

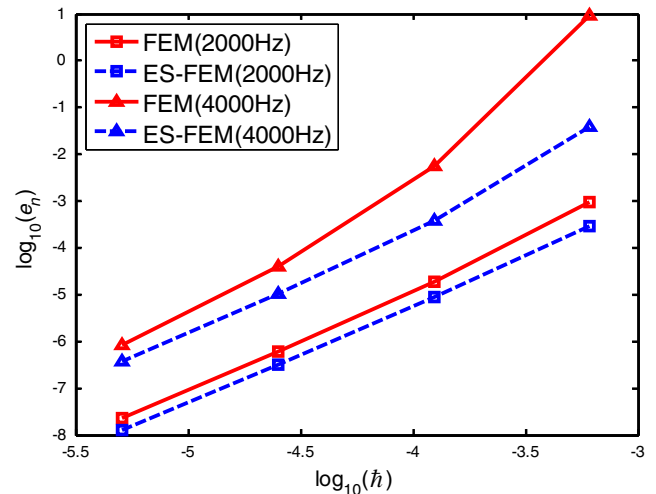


Fig. 6. Comparison of convergence rate of the solutions obtained using FEM and the ES-FEM at different frequency.

Table 1
Comparison of the solutions of acoustic pressure along the ξ -axis with frequency 2000 Hz.

| Coordinates [x_1, x_2] (m) | ES-FEM | FEM | Exact solutions | Local error e_p (%) 2000 Hz | |
|--------------------------------|-----------|-----------|-----------------|-------------------------------|-------|
| | | | | ES-FEM | FEM |
| (0.1, 0.0) | -5.61E+06 | -6.05E+06 | -5.35E+06 | 0.048 | 0.131 |
| (0.2, 0.0) | -1.59E+07 | -1.57E+07 | -1.58E+07 | 0.004 | 0.010 |
| (0.3, 0.0) | -1.57E+07 | -1.51E+07 | -1.58E+07 | 0.008 | 0.049 |
| (0.4, 0.0) | -5.15E+06 | -4.61E+06 | -5.35E+06 | 0.037 | 0.138 |
| (0.5, 0.0) | 8.78E+06 | 8.84E+06 | 8.66E+06 | 0.014 | 0.021 |
| (0.6, 0.0) | 1.69E+07 | 1.65E+07 | 1.69E+07 | 0.001 | 0.025 |
| (0.7, 0.0) | 1.39E+07 | 1.34E+07 | 1.40E+07 | 0.007 | 0.042 |
| (0.8, 0.0) | 1.74E+06 | 1.56E+06 | 1.81E+06 | 0.040 | 0.141 |
| (0.9, 0.0) | -1.16E+07 | -1.13E+07 | -1.16E+07 | 0.000 | 0.023 |
| (1.0, 0.0) | -1.72E+07 | -1.68E+07 | -1.73E+07 | 0.006 | 0.030 |

Table 2
Comparison of the solutions of acoustic pressure along the ξ -axis with frequency 4000 Hz.

| Coordinates [x_1, x_2] (m) | ES-FEM | FEM | Exact solutions | Local error e_p (%) 4000 Hz | |
|--------------------------------|-----------|-----------|-----------------|-------------------------------|-------|
| | | | | ES-FEM | FEM |
| (0.1, 0.0) | -1.44E+07 | -1.38E+07 | -1.40E+07 | 0.025 | 0.016 |
| (0.2, 0.0) | 1.48E+07 | 2.44E+07 | 1.16E+07 | 0.279 | 1.104 |
| (0.3, 0.0) | 1.17E+07 | 1.09E+07 | 1.16E+07 | 0.008 | 0.057 |
| (0.4, 0.0) | -1.69E+07 | -2.57E+07 | -1.40E+07 | 0.209 | 0.832 |
| (0.5, 0.0) | -8.61E+06 | -7.91E+06 | -8.66E+06 | 0.006 | 0.086 |
| (0.6, 0.0) | 1.85E+07 | 2.66E+07 | 1.58E+07 | 0.169 | 0.681 |
| (0.7, 0.0) | 5.26E+06 | 4.79E+06 | 5.35E+06 | 0.018 | 0.105 |
| (0.8, 0.0) | -1.94E+07 | -2.72E+07 | -1.69E+07 | 0.148 | 0.603 |
| (0.9, 0.0) | -1.73E+06 | -1.60E+06 | -1.81E+06 | 0.043 | 0.114 |
| (1.0, 0.0) | 1.95E+07 | 2.73E+07 | 1.73E+07 | 0.125 | 0.579 |

$$p = -j\rho c v_n \frac{\cos(\kappa(1-\xi))}{\sin(\kappa)}, \tag{41}$$

$$v = \frac{v_n \sin(\kappa(1-\xi))}{\sin(\kappa)}. \tag{42}$$

The 2D tube with rigid walls has eigenmodes corresponding to the values:

$$f = \frac{c}{2} \sqrt{\left(\frac{m}{L}\right)^2 + \left(\frac{n}{b}\right)^2} \quad m = 0, 1, 2, \dots, n = 0, 1, 2, \dots \tag{43}$$

f here are the eigenfrequencies of this problem, m and n can not be zero simultaneously. Note that in the vicinity of the above values, the problem becomes numerically ill-posed, which significantly increases the numerical error.

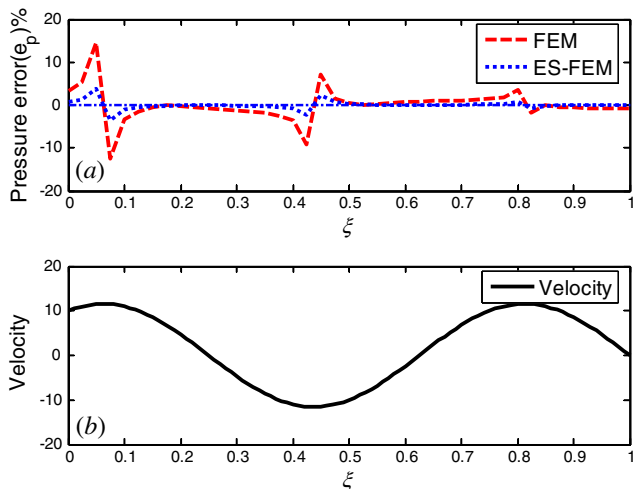


Fig. 7. (a) Local relative error in acoustic pressure obtained using the ES-FEM and the FEM (b) velocity along ξ -axis (2000 Hz).

5.2.1. Convergence study

The convergence property is investigated by employing four models with 103, 365, 1369 and 5297 uniformly distributed nodes. Fig. 6 presents the convergence curves in terms of global error against the non-dimensional mesh size h at frequency of 2000 Hz and 4000 Hz for both ES-FEM and FEM simulations. From these figures, it can be observed that the present ES-FEM and FEM give similar convergence rate but the former produces more accurate results than the latter does.

5.2.2. Accuracy of acoustic field

The numerical solutions of acoustic pressure using ES-FEM and FEM along the x -axis at frequency of 2000 Hz ($\kappa = 8.38$) and 4000 Hz ($\kappa = 16.76$) are presented in Tables 2 and 3. Both FEM

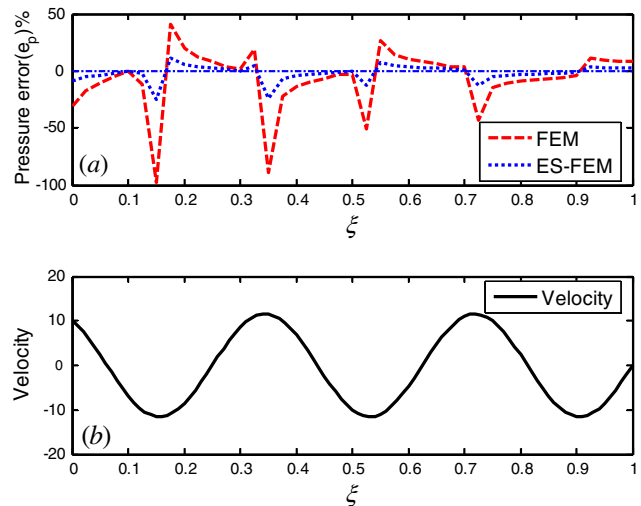


Fig. 8. (a) Local relative error in acoustic pressure obtained using the ES-FEM and the FEM (b) velocity along ξ -axis (4000 Hz).

Table 3

2D tube natural eigenfrequencies calculated by FEM and ES-FEM.

| Eigenvalue | Exact (Hz) | FEM (Hz) | Error of FEM (%) | ES-FEM (Hz) | Error of ES-FEM (%) | Error of FEM Error of ES-FEM |
|------------|------------|----------|------------------|-------------|---------------------|---------------------------------|
| 1 | 750.00 | 750.22 | 0.029333 | 750.00 | 0.000000 | – |
| 2 | 1500.00 | 1501.80 | 0.120000 | 1500.00 | 0.000000 | – |
| 3 | 2250.00 | 2256.10 | 0.271111 | 2250.10 | 0.004444 | 61.00000 |
| 4 | 3000.00 | 3014.50 | 0.483333 | 3000.30 | 0.010000 | 48.33333 |
| 5 | 3750.00 | 3778.30 | 0.754667 | 3750.60 | 0.016000 | 47.16667 |
| 6 | 4500.00 | 4549.20 | 1.093333 | 4501.00 | 0.022222 | 49.20000 |
| 7 | 5250.00 | 5328.50 | 1.495238 | 5251.60 | 0.030476 | 49.06250 |
| 8 | 6000.00 | 6117.80 | 1.963333 | 6002.30 | 0.038333 | 51.21739 |
| 9 | 6750.00 | 6918.80 | 2.500741 | 6753.30 | 0.048889 | 51.15152 |
| 10 | 7500.00 | 7733.20 | 3.109333 | 7504.60 | 0.061333 | 50.69565 |
| 11 | 7500.00 | 7836.20 | 4.482667 | 7582.00 | 1.093333 | 4.10000 |
| 12 | 7537.40 | 7878.30 | 4.522780 | 7618.40 | 1.074641 | 4.20864 |
| 13 | 7648.50 | 8004.30 | 4.651893 | 7726.90 | 1.025038 | 4.53827 |
| 14 | 7830.20 | 8211.00 | 4.863222 | 7904.50 | 0.948890 | 5.12517 |
| 15 | 8077.70 | 8494.00 | 5.153695 | 8147.00 | 0.857917 | 6.00722 |
| 16 | 8250.00 | 8562.90 | 3.792727 | 8256.10 | 0.073939 | 51.29508 |
| 17 | 8385.30 | 8848.00 | 5.517990 | 8448.80 | 0.757278 | 7.28661 |
| 18 | 8746.40 | 9267.30 | 5.955593 | 8804.20 | 0.660843 | 9.01211 |
| 19 | 9000.00 | 9409.70 | 4.552222 | 9007.90 | 0.087778 | 51.86076 |
| 20 | 9154.90 | 9746.60 | 6.463205 | 9207.30 | 0.572371 | 11.29198 |
| 21* | 9604.70 | 10276.00 | 6.989286 | 9652.50 | 0.497673 | 14.04393 |
| 22* | 9750.00 | 10281.00 | 5.446154 | 9760.00 | 0.102564 | 53.10000 |
| 23* | 10090.00 | 10866.00 | 7.690783 | 10134.00 | 0.436075 | 17.63636 |
| 24* | 10500.00 | 11164.00 | 6.323810 | 10512.00 | 0.114286 | 55.33333 |
| 25* | 10607.00 | 11499.00 | 8.409541 | 10649.00 | 0.395965 | 21.23810 |

* The frequencies do not satisfy the rule of thumb of the relation between the frequency and mesh size.

and ES-FEM are solved with same number of triangular mesh. To demonstrate more clearly, a local relative error in acoustic pressure e_p is defined as

$$e_p = \frac{|p^{exact} - p^h|}{p^{exact}} \times 100\%. \tag{44}$$

The local relative errors in acoustic pressure are computed for ES-FEM and FEM models and listed in the Tables 1 and 2. It can be clearly observed from Tables 1 and 2 that: (a) the present ES-FEM solutions are in good agreement with the exact solutions and these results again validate the ES-FEM model. (b) The local relative errors in acoustic pressure become larger with the increase of frequency for both methods, but the ES-FEM obtains much more accurate results than the FEM does at the same frequency.

The reason why the ES-FEM can give much more accurate results than the FEM will be further investigated in detail. A comparison between the ES-FEM and FEM for the local relative errors (e_p) along the x -axis is given in Figs. 7 and 8a at the frequency of 2000 Hz ($\kappa = 8.38$) and 4000 Hz ($\kappa = 16.76$), while the acoustic particle velocity linked to the gradient of acoustic pressure are presented in Figs. 7 and 8b at these two different frequency values. As depicted in these figures, the peak of local relative errors for ES-FEM and FEM both occur where the velocity (or gradient of acoustic pressure) is the maximum (both 2000 Hz and 4000 Hz). However, the local relative errors of ES-FEM are much smaller than the corresponding FEM. It is well-known that the linear FEM using triangular elements produces constant gradient field which will lead to inaccurate gradient solutions, especially in high-gradient regions; while the ES-FEM can give better results owing to the

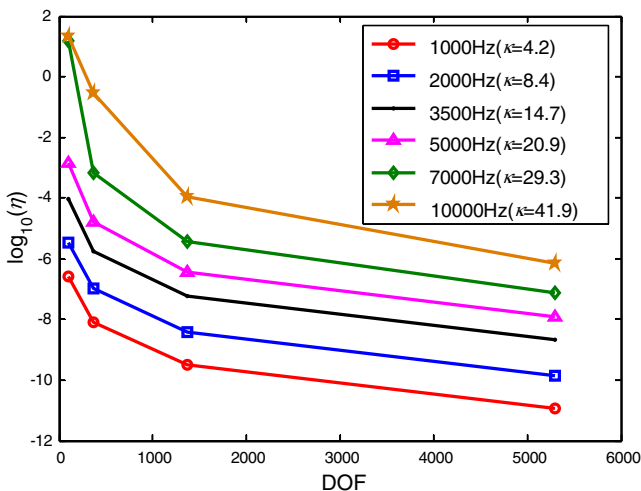


Fig. 9. The relative error at different frequency values obtained using the ES-FEM.

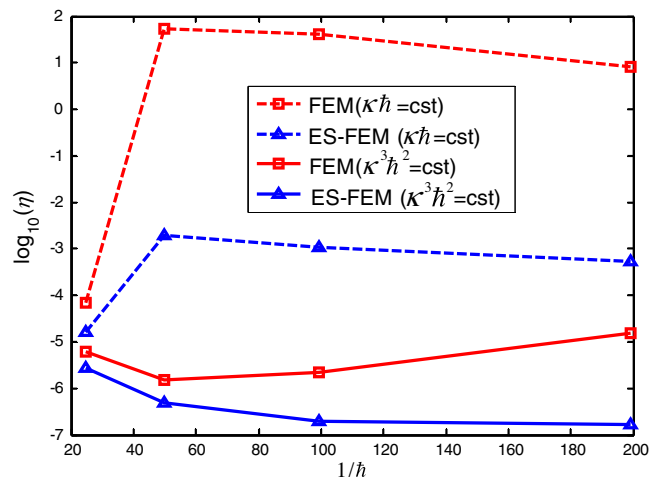


Fig. 10. Comparison of relative error obtained using the linear FEM and the ES-FEM by keeping κh and $\kappa^3 h^2$ constant.

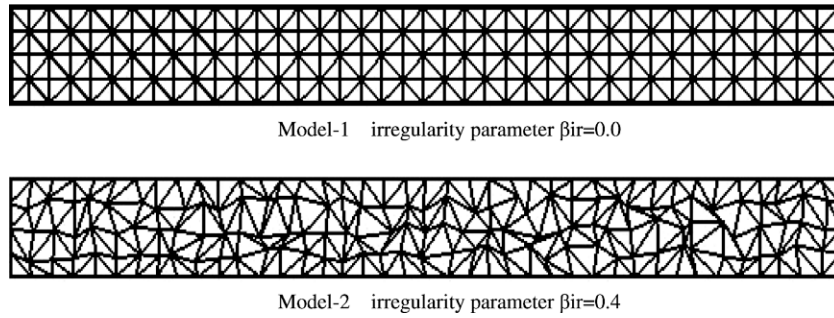


Fig. 11. Two meshes of regular and irregular 205 nodes for a chamber of $L = 1$ m and $H = 0.1$ m generated with different nodal irregularity parameter.

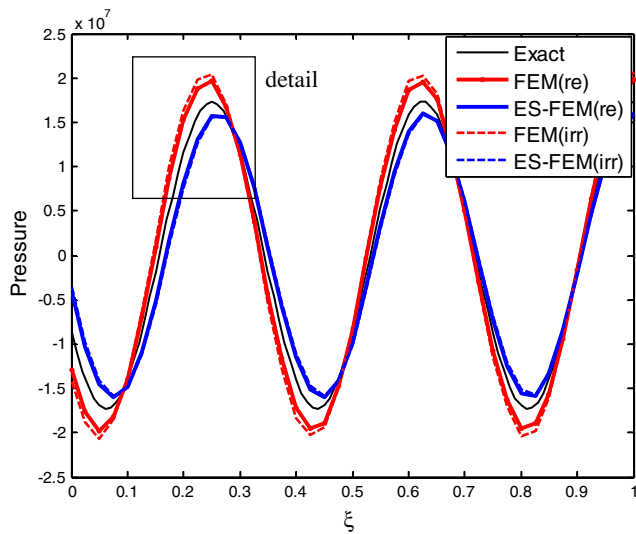
edge-based gradient smoothing operation which can soften the structure and provide a properly softened stiffness to the acoustic model.

5.2.3. Acoustic eigenfrequencies analysis

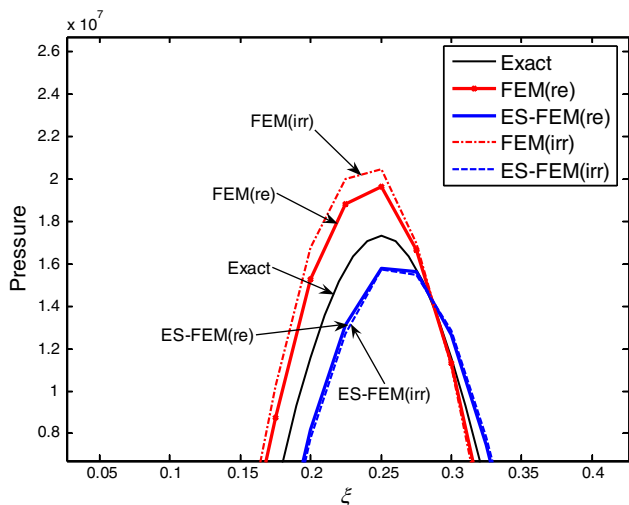
Acoustic analysis is now almost routinely performed in the development of engineering structures (the car passenger com-

partment and aircraft cabin, etc.), because of the increased awareness of enclosure sound quality. The acoustic performance of these products can be investigated in the design stage by analyzing the modal quantities, i.e., eigenfrequencies, eigenmodes. It is known that the FEM model behaviors more stiff than the continuum counterpart, resulting in a higher predicted eigenfrequencies in acoustic analysis. So the acoustic eigenfrequencies analysis using ES-FEM and FEM has been conducted in this section.

The tube is discretized with average mesh size of 0.025m which satisfies the “the rule of thumb” guarantee a frequency limit of 9554 Hz. Table 3 lists the first twenty-five natural eigenfrequencies obtained from ES-FEM and FEM with the same mesh. The analytical solutions are also listed in the table. As indicated in Table 3, for low eigenfrequencies, the ES-FEM model can provide much more accurate eigenfrequencies prediction than the FEM model. For higher eigenfrequencies, the shift between the numerical eigenfrequencies of FEM and the analytical becomes much larger, while the present ES-FEM still gives very accurate solution. This numerical example also validates that ES-FEM behaves much softer than the overly-stiff FEM model and the softened stiffness is much closer to the continuous system.

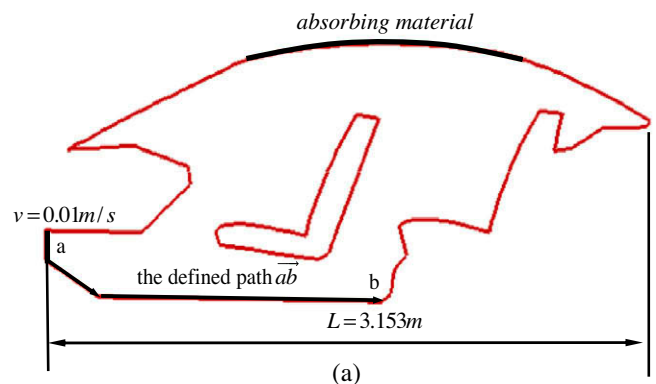


(a) Full scale distribution

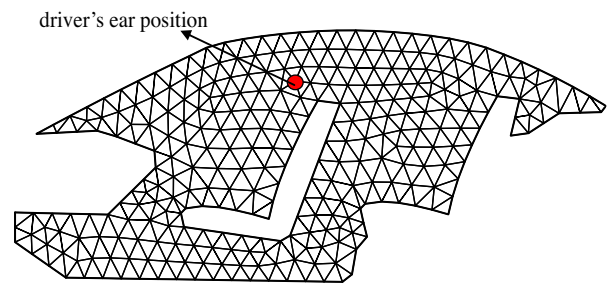


(b) Zoomed-in distribution

Fig. 12. Acoustic pressure distribution obtained using ES-FEM and FEM along the ξ -axis (4000 Hz).



(a)



(b)

Fig. 13. (a) Acoustic problem for a 2D car boundary condition, the results on \overline{ab} path will be closely examined, and (b) mesh.

5.2.4. Relative error and control for ES-FEM

To investigate the relative error according to the definition in Eq. (34) of present ES-FEM, four types of uniform mesh (103, 365, 1369, 5297 nodes, respectively) are employed. The results of ES-FEM for several frequency values are plotted in Fig. 9. As shown in this figure, at lower frequency values, the relative error is small even though the mesh size is large; with the increase of frequency value, the relative error increases obviously compared to that of the lower frequency with the same mesh. It means that a certain level of error should be controlled using more nodes for the ES-FEM at high frequency. Therefore the relation of non-dimensional κ and mesh size h is studied in more detail in order to control the relative error of ES-FEM. Based on Eq. (35), the control of the numerical error is related to the control of the non-dimensional terms κh and $\kappa^3 h^2$. Keeping κh constant by varying wave number and mesh size under the condition $\kappa h < 1$, the relative error will increase linearly with wave number κ due to the term $\kappa^3 h^2$. While keeping $\kappa^3 h^2$ constant by varying wave number and mesh size, the

relative error depends only on the interpolation error and hence can be controlled. A test to show this is conducted using both ES-FEM and FEM by keeping κh and $\kappa^3 h^2$ constant.

A comparison between the ES-FEM and FEM relative errors is shown in Fig. 10 by keeping κh and $\kappa^3 h^2$ constant. As indicated in the figure, keeping $\kappa^3 h^2$ constant, both ES-FEM and FEM can give acceptable results, while the result of ES-FEM is improved significantly; keeping κh constant, the relative errors of both ES-FEM and FEM increase noticeably but the present ES-FEM is less sensitive to wave number than the FEM. It can be concluded that keeping $\kappa^3 h^2$ constant is more sufficient to obtain acceptable results for both ES-FEM and FEM models, and the present ES-FEM is more stable than FEM by keeping κh or $\kappa^3 h^2$ constant.

5.2.5. Effects of nodal irregularity

To evaluate the influence of the mesh irregularities on the accuracy, the numerical example about regular mesh and irregular mesh will be tested. The irregularly distributed nodes are

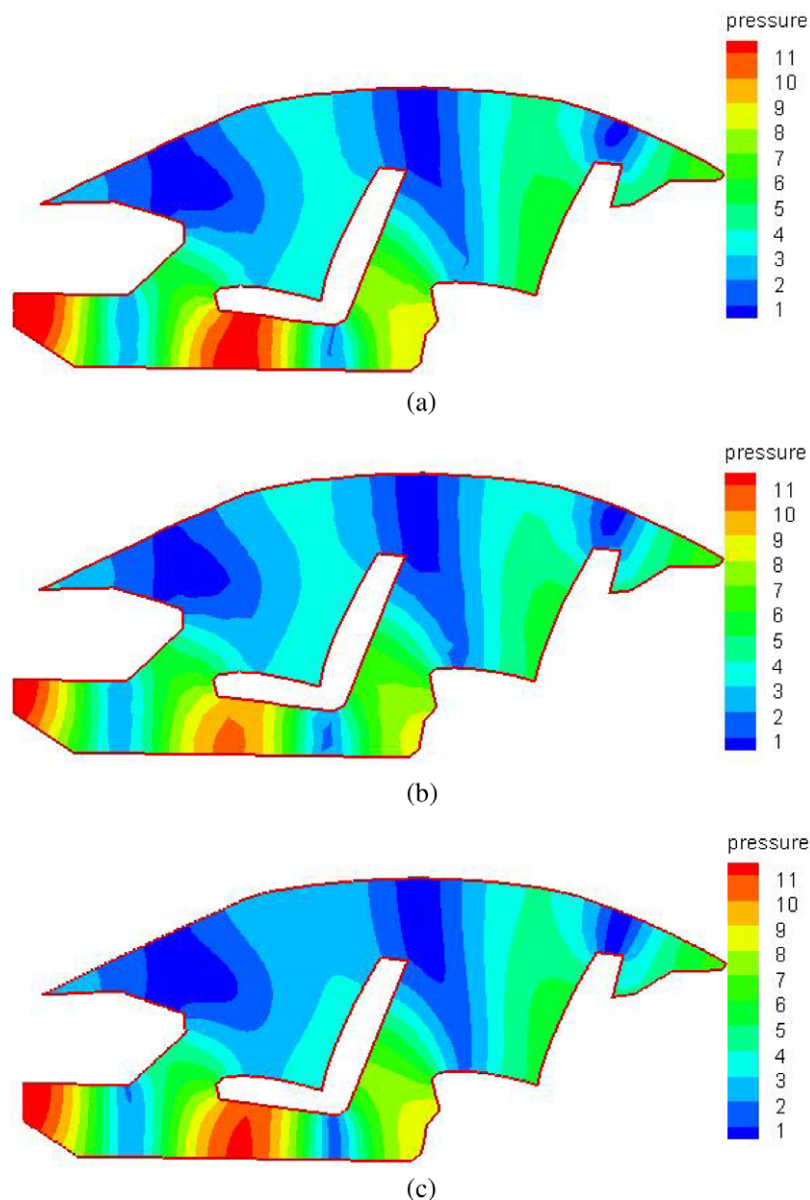


Fig. 14. (a) Acoustic pressure distribution obtained using ES-FEM (200 Hz). (b) Acoustic pressure distribution obtained using FEM (200 Hz). (c) Acoustic pressure distribution obtained using FEM with 22524 nodes (200 Hz).

generated based on nodal irregularity degree defined in the following expression:

$$\begin{aligned} x' &= x + \Delta x \cdot r_c \cdot \beta_{ir}, \\ y' &= y + \Delta y \cdot r_c \cdot \beta_{ir}, \end{aligned} \quad (45)$$

where x' and y' are the coordinates of the irregular mesh, x and y are original regular coordinates, Δx and Δy are the initial regular nodal spacing in x - and y -directions, r_c is a computer-generated random

number between -1.0 and 1.0 , and β_{ir} is a prescribed irregularity degree whose value is varied between 0.0 and 0.5 . A bigger value of β_{ir} leads to more irregular nodes distribution to be used in the nodal irregularity study. Fig. 11 presents the result of two mesh models of different nodal irregularity.

The study is performed at the frequency of 4000 Hz with two types of mesh. The acoustic pressure distributions computed using the ES-FEM along the x -axis are plotted in Fig. 12a and b together with the *exact* solution. For the purpose of comparison, the FEM

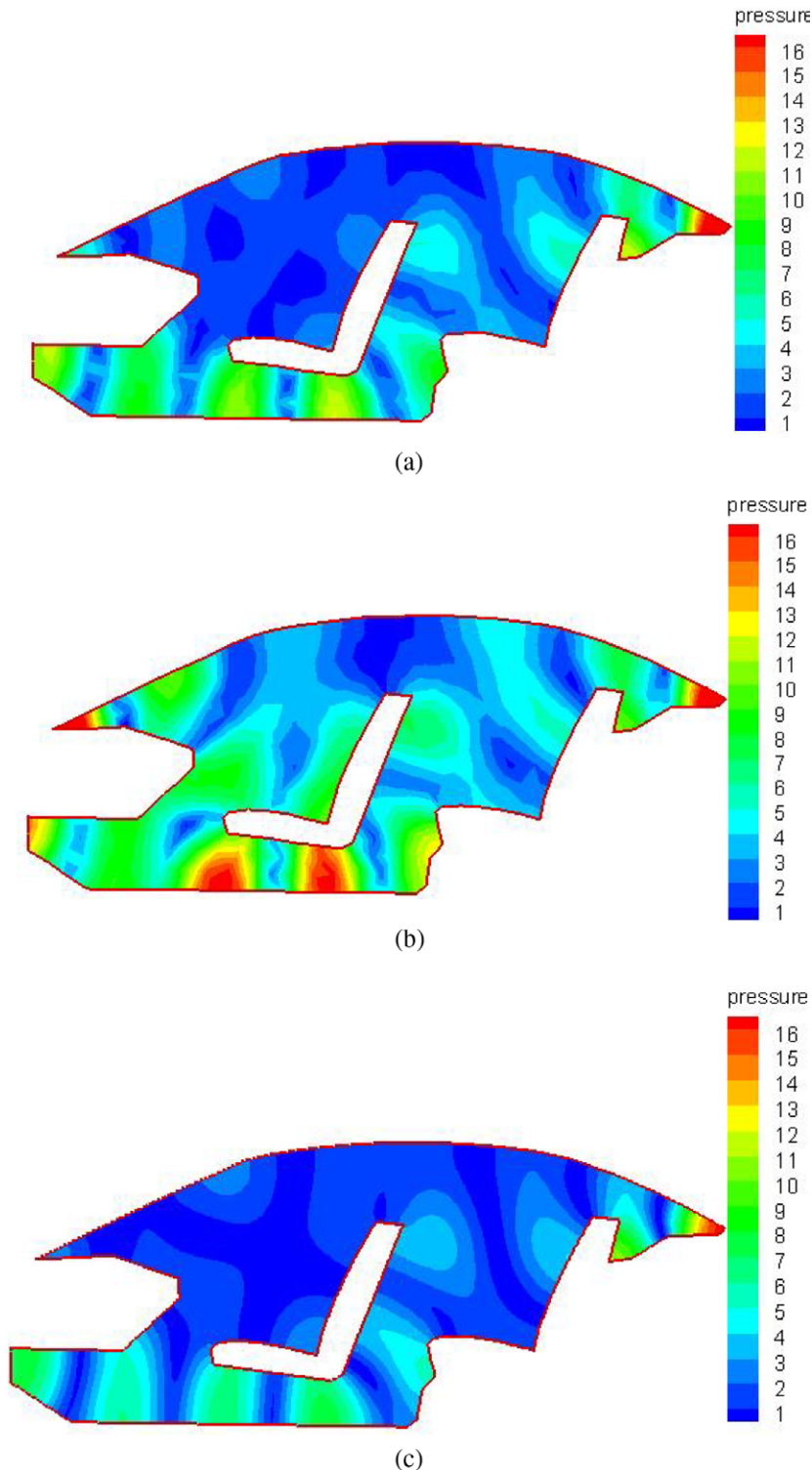


Fig. 15. (a) Acoustic pressure distribution obtained using ES-FEM (400 Hz). (b) Acoustic pressure distribution obtained using FEM (400 Hz). (c) Acoustic pressure distribution obtained using FEM with 22524 nodes (400 Hz).

results are also presented. The pictures show that the FEM results will become worse when the irregular meshes are used. However, the accuracy of ES-FEM solutions changes only a little when the irregular arrangement nodes switch to regular arrangement nodes. These crucial findings imply that the present ES-FEM works well even with the extremely distorted cells. The FEM, however, is known and confirmed here being sensitive to mesh distortions.

5.3. 2D car acoustic problem

We now consider a problem of analyzing the acoustic pressure distribution in a car passenger compartment [27], where one of the main sources generating the noise in the passenger compartment is engine vibration. The geometry of the passenger compartment is approximately considered as prismatic and it is possible to simplify the three dimensional to two-dimensional. Fig. 13a illustrates the 2D geometry of the problem domain. The front panel of the passenger compartment is subjected to the vibration coming from the engine with the velocity of 0.01 m/s. The roof of the passenger compartment is fixed with absorbing material with admittance of 0.00144 m/(Pa s). The frequency values of 200 Hz and 400 Hz will be studied in the model.

Fig. 13b shows the distribution of 305 nodes with the average spacing of 0.1 m, which can satisfy “the rule of thumb” for the considered frequency values. Figs. 14 and 15a are acoustic pressure distributed in the passenger compartment at 200 Hz and 400 Hz obtained from the ES-FEM, while the results using the FEM at 200 Hz and 400 Hz are plotted in Figs. 14 and 15b, respectively. Because the analytical solution is unavailable for this problem, a reference configuration using FEM with a very fine mesh (22,524 nodes) is adopted and the results at 200 Hz and 400 Hz are plotted in Figs. 14 and 15c.

From these figures, it is found that the contours of the pressure obtained from ES-FEM and FEM are similar compared with the reference solution in the same scale for 200 Hz. When it comes to higher frequency ($f = 400$ Hz), the contour of the pressure obtained from the ES-FEM does not deviate much from the reference result, while the result from the FEM has been affected significantly by higher frequency and departs a lot from the reference result. To show the results quantitatively for these two frequency values, the real part of pressure obtained from the ES-FEM and FEM along the defined path ab shown in Fig. 13a are given in Fig. 16a and b, respectively. The errors of the real part of the pressure obtained from the ES-FEM and FEM along the defined path ab are similar to the reference result at the frequency of 200 Hz, while when the frequency is 400 Hz, the real part of acoustic pressure obtained from the ES-FEM along the defined path ab varies a little from the reference result, but much less than that of FEM.

Then the direct frequency response analysis is conducted using present ES-FEM and FEM. The frequency response analysis solves Eq. (15) for the selected frequencies. At each frequency, the system equations are set up and solved to obtain the pressure distribution $\{P\}$. The boundary conditions for this 2D car problem are the same as previous one including the Neumann and Admittance boundary conditions. The average mesh size is 0.1 m which gives frequency limit of 541 Hz. A full range frequency sweep is done from 1 Hz to 800 Hz at intervals of 1.0 Hz and the response (sound pressure level) at the driver’s ear point, illustrated in Fig. 13b is measured. The results using ES-FEM and FEM are depicted in Fig. 17. As the analytical solution is unavailable, the reference solution using FEM with 22,524 nodes is also provided. As shown in the figure, the ES-FEM can provide much better result than FEM in the full frequency range. We also note that when the frequency exceeds 541 Hz which is the limit of the FEM based on the rule of thumb, a deviation between the ES-FEM and the reference result can also be observed, but the present ES-FEM can still give more accurate

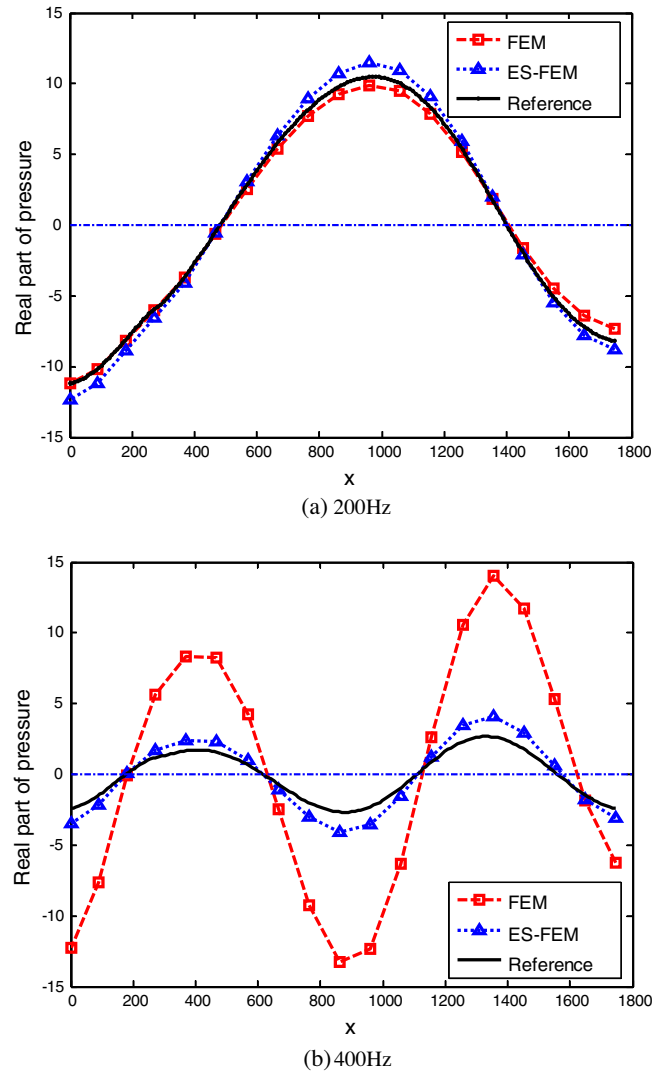


Fig. 16. Real part of acoustic pressure distribution along the path ab shown in Fig. 14.

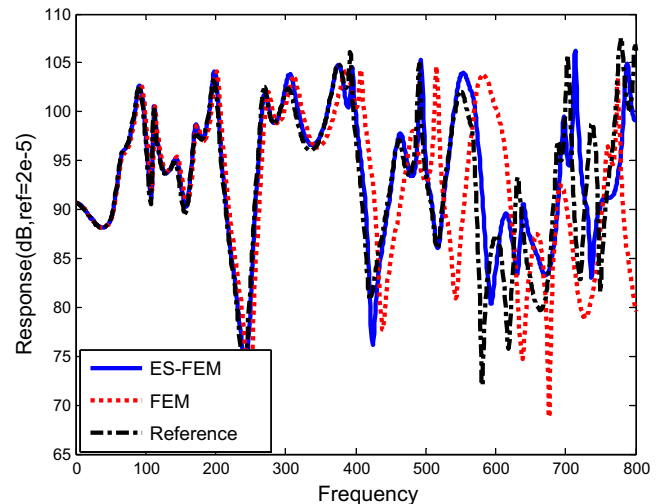


Fig. 17. Acoustic frequency response at driver’s ear for the 2D car problem obtained using ES-FEM and FEM using the same mesh.

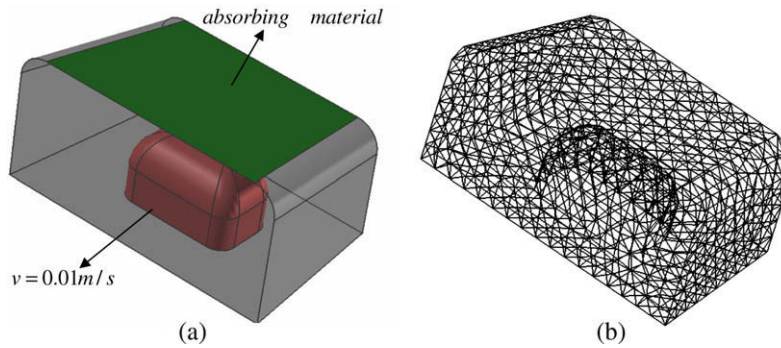


Fig. 18. 3D acoustics in an engine chamber (a) CAD model (b) mesh of tetrahedrons.

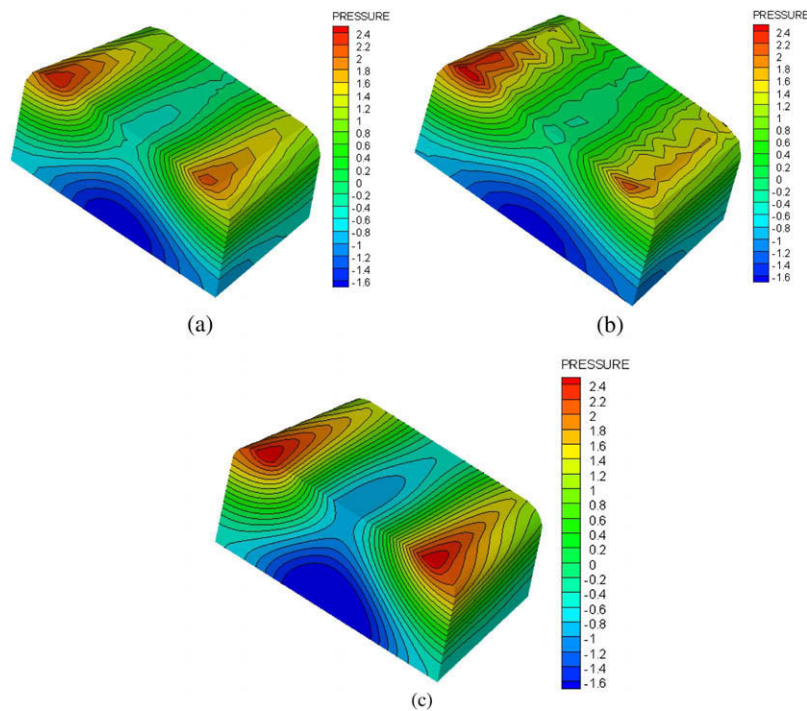


Fig. 19. Real part of acoustic pressure distribution: (a) ES-FEM (b) FEM (c) Reference (frequency = 400 Hz).

solutions compared with FEM. This numerical example validates that ES-FEM with softened stiffness can give very accurate solution even at high frequencies.

5.4. 3D engine chamber problem

Due to the excellent features of ES-FEM confirmed by the 2D problems, we have further developed a 3D code. This 3D numerical example is developed to analyze the acoustical pressure distribution in an engine chamber. The vibration of the engine is found to be a major noise source. The model is described in Fig. 18, the engine is located at the bottom center of the field and the velocity of vibration surface is 0.01 m/s, the absorbing material is attached to the engine hood and the admittance is set at 0.00144 m/(Pa s). The model is discretized with 1211 node with average node spacing of 0.05 m. This 3D example is studied using both FEM and ES-FEM with a frequency of 400 Hz. A similar example has been studied in [28].

The acoustic pressure distribution of ES-FEM versus FEM with 1211 nodes are plotted in Fig. 19a and b, respectively. The reference result obtained from the FEM with a very fine mesh (21197 nodes) is also plotted in Fig. 19c. These figures show that for this

3D case the contour lines of ES-FEM solution are closer to the reference solution and much smoother than that of FEM result, especially in high-gradient domains.

6. Conclusions and discussions

In this work, the edge-based smoothed finite element (ES-FEM) is further formulated for solving acoustic problems in 2D and 3D domains. The smoothed Galerkin weak form is adopted to formulate the discretized system equations and the numerical integration is performed based on the smoothing domains associated with the edges of the triangles in 2D or surfaces of tetrahedrons in 3D. A number of acoustic problems are investigated in detail to study the accuracy, convergence and error control of the ES-FEM. The following conclusion can be derived as:

- (a) The ES-FEM using triangular elements in 2D space and tetrahedral elements in 3D space is very simple; no additional parameters or degrees of freedoms are needed, and the method can be implemented in a straightforward way with little change to the FEM code.

- (b) The ES-FEM is less sensitive to the wave number and can achieve higher accuracy than the FEM does, especially for higher wave numbers. The ES-FEM can also provide much better frequency response solution and natural eigenfrequencies prediction in acoustic analysis. This is due to the edge-based gradient smoothing technique used in the ES-FEM providing a properly softened stiffness to the model.
- (c) The ES-FEM is not sensitive to distortion of element.
- (d) For the practical acoustic problems with complicated domains and boundary conditions, the ES-FEM obtains much more accurate results than the FEM does with the same mesh. It indicates that the present ES-FEM has great potential in the practical analysis of acoustic problems.

Acknowledgements

The author wish to thank the support of the China-funded Post-graduates' Studying Aboard Program for Building Top University and the National Natural Science Foundation of China. This work is partially supported by A*Star, Singapore. It is also partially supported by the Open Research Fund Program of the State Key Laboratory of Advanced Technology of Design and Manufacturing for Vehicle Body, Hunan University, PR China under the grant number 40915001.

References

- [1] S. Suleau, A. Deraemaeker, Ph. Bouillard, Dispersion and pollution of meshless solution for the Helmholtz equation, *Comput. Meth. Appl. Mech. Engrg.* 190 (2000) 639–657.
- [2] I. Harari, F. Magoulès, Numerical investigations of stabilized finite element computations for acoustics, *Wave Motion* 39 (2004) 339–349.
- [3] A. Deraemaeker, I. Babuska, Ph. Bouillard, Dispersion and pollution of the FEM solution for the Helmholtz equation in one, two and three dimension, *Int. J. Numer. Meth. Engrg.* 46 (1999) 471–499.
- [4] S. Petersen, D. Dreyer, O.v. Estorff, Assessment of finite and spectral element shape functions or efficient iterative simulations of interior acoustics, *Comput. Meth. Appl. Mech. Engrg.* 195 (2006) 6463–6478.
- [5] L. Thompson, P. Pinsky, A Galerkin least-squares finite element method for the two-dimensional Helmholtz equation, *Int. J. Numer. Meth. Engrg.* 38 (1995) 371–397.
- [6] Guasch, R. Codina, An algebraic subgrid scale FEM for the convected Helmholtz equation in two dimension with applications in aeroacoustics, *Comput. Meth. Appl. Mech.* 196 (2007) 4672–4689.
- [7] T. Belytschko, Y.Y. Lu, L. Gu, Element-free Galerkin methods, *Int. J. Numer. Meth. Engrg.* 37 (1994) 229–256.
- [8] Ph. Bouillard, S. Suleau, Element-free Galerkin solutions for Helmholtz problems: formulation and numerical assessment of the pollution effect, *Comput. Meth. Appl. Mech. Engrg.* 162 (1998) 317–335.
- [9] G.B. Alvarez, A.F.D. Loula, E.G.D.d. Carmo, F.A. Rochinha, A discontinuous finite element formulation for Helmholtz equation, *Comput. Meth. Appl. Mech. Engrg.* 195 (2006) 4018–4035.
- [10] J.S. Chen, C.T. Wu, S. Yoon, Y. You, A stabilized conforming nodal integration for Galerkin meshfree methods, *Int. J. Numer. Meth. Engrg.* 50 (2001) 435–466.
- [11] J.W. Yoo, B. Moran, J.S. Chen, Stabilized conforming nodal integration in the natural-element method, *Int. J. Numer. Meth. Engrg.* 60 (2004) 861–890.
- [12] G.R. Liu, Y.T. Gu, A point interpolation method for two-dimensional solids, *Int. J. Numer. Meth. Engrg.* 50 (2001) 937–951.
- [13] G.R. Liu, *Meshfree Methods: Moving Beyond the Finite Element Method*, 2 ed., CRC Press, Boca Raton, USA, 2009.
- [14] G.R. Liu, A generalized gradient smoothing technique and the smoothed bilinear form for Galerkin formulation of wide class of computational methods, *Int. J. Computat. Meth.* 5 (2008) 199–236.
- [15] G.R. Liu, G.Y. Zhang, Upper bound solution to elasticity problems: a unique property of the linearly conforming point interpolation method (LC-PIM), *Int. J. Numer. Meth. Engrg.* 74 (2008) 1128–1161.
- [16] G.R. Liu, T.T. Nguyen, X.H. Nguyen, K.Y. Lam, A node-based smoothed finite element method (NS-FEM) for upper bound solution to solid mechanics problems, *Comput. Struct.* 87 (2009) 14–26.
- [17] G.R. Liu, T.T. Nguyen, K.Y. Lam, An edge-based smoothed finite element method (ES-FEM) for static free, and forced vibration analysis, *J. Sound Vib.* 320 (2009) 1100–1130.
- [18] G.R. Liu, G.Y. Zhang, Edge-based smoothed point interpolation method, *Int. J. Computat. Meth.* 5 (2008) 621–646.
- [19] G.R. Liu, T.T. Nguyen, K.Y. Lam, A novel alpha finite element method (aFEM) for exact solution to mechanics problems using triangular and tetrahedral elements, *Comput. Meth. Appl. Mech. Engrg.* (2008), doi:10.1016/j.cma.2008.03.011.
- [20] T.T. Nguyen, G.R. Liu, K.Y. Lam, G.Y. Zhang, A face-based smoothed finite element method (FS-FEM) for 3D linear and nonlinear solid mechanics problems using 4-node tetrahedral elements, *Int. J. Numer. Meth. Engrg.* 78 (2009) 324–353.
- [21] X.Y. Cui, G.R. Liu, G.Y. Li, G.Y. Zhang, G. Zheng, Analysis of plates and shells using an edge-based smoothed finite element method, *Comput. Mech.* (2009), doi:10.1007/s00466-009-0429-9.
- [22] K.Y. Dai, G.R. Liu, T.T. Nguyen, An n-sided polygonal smoothed finite element method (nSFEM) for solid mechanics, *Finite Elem. Anal. Des.* 43 (2007) 847–860.
- [23] F. Ihlenburg, I. Babuška, Reliability of finite element methods for the numerical computation of waves, *Adv. Engrg. Software* 28 (1997) 417–424.
- [24] S. Irimie, Ph. Bouillard, A residual a posteriori error estimator for the finite element solution of the Helmholtz equation, *Comput. Meth. Appl. Mech. Engrg.* 190 (2001) 2027–2042.
- [25] F. Ihlenburg, I. Babuška, Finite element solution of the Helmholtz equation with high wave number. Part I: The h-version of the FEM, *Comput. Math. Appl.* 30 (9) (1995) 9–37.
- [26] D.J. Nefske, J.A. Wolf Jr., L.J. Howell, Structural-acoustic finite element analysis of the automobile passenger compartment: a review of current practice, *J. Sound Vib.* 80 (2) (1982) 247–266.
- [27] Ph. Bouillard, V. Lacroix, E. De Bel, A wave-oriented meshless formulation for acoustical and vibro-acoustical applications, *Wave Motion* 39 (2004) 295–305.
- [28] J.F. Deu, W. Larbi, R. Ohayon, Piezoelectric structural acoustic problems; symmetric variational formulation and finite elements, *Comput. Meth. Appl. Mech. Engrg.* 197 (2008) 1715–1724.